13

Model of physical sputtering of amorphous materials

© A.E. Pestov, M.S. Mikhailenko, A.K. Chernyshev, M.V. Zorina, N.I. Chkhalo

Institute of Physics of Microstructures, Russian Academy of Sciences,
607680 Nizhny Novgorod, Russia
e-mail: mikhaylenko@ipmras.ru

The paper demonstrates the pulse mechanism of physical sputtering taking into account the evolution of the surface. The model is based on pulsed energy transfer in collision cascades. The main feature is the consideration of surface roughness. The results of numerical simulation qualitatively coincide with those observed in experiments. It is shown that the angular dependences calculated in the framework of this model have closer values of the sputtering yields to the experimental ones than those calculated in TRIM.

Keywords: ion etching, numerical simulation, roughness, Monte Carlo.

DOI: 10.21883/TP.2022.08.54571.84-22

Introduction

Ion-beam surface treatment (correction of local shape errors, ion polishing and aspherization) is considered as one of the main techniques of finishing the surface of optical elements. With its help, it is possible to obtain optical surfaces, including aspherical ones, with shape accuracy at the RMS parameter level at the level of 1 nm and with a roughness better than 0.3 nm [1–3]. A number of approaches have been developed that simulate the interaction of an ion beam with a surface and predict various parameters of the interaction of accelerated ions with an amorphous target (sputtering coefficient, depth and distribution of implanted ions, density of ion-induced defects, etc.). Most of these approaches are based on the classical work of Sigmund [4], which is based on the solution of the kinetic Boltzmann equation, but, as a rule, they do not consider the effect of ion etching on the surface, i.e. they do not describe the erosion of the surface, the development of roughness, etc. While in the ion-beam processing of optical elements, the main attention should be paid to the roughness. The present work is aimed at constructing a model (SPnSurface) that allows predicting the dynamics of the morphology of the surface of amorphous materials during irradiation with an accelerated ion beam.

1. Mathematical model

Quantitatively, physical atomization is described by the atomization coefficient Y, which is a statistical value and is expressed

$$Y = \frac{Count\ of\ ejected\ atoms}{Count\ of\ incident\ particles}. \quad (1)$$

Currently, the pulsed mechanism of destruction of the surface of a solid under the action of ion bombardment is generally recognized. In this case, the exchange of pulses occurs when the bombarding ion collides with the lattice atoms and the lattice atoms among themselves. As an initial approximation, we consider the classical model of elastic scattering of two particles in the field of central forces. An example of such scattering is shown in Fig. 1.

In this case, the energy transferred by the incoming particle with energy E to the target particle can be represented in the form

$$T = \gamma E \sin^2 \frac{\Theta}{2}, \quad (2)$$

where Θ is the scattering angle of the center of mass in a system of two particles, and γ is the energy transfer coefficient:

$$\gamma = \frac{4M_1 M_2}{(M_1 + M_2)^2}, \quad (3)$$

where $M1$ and $M2$ — are the atomic masses of the incoming particle and target, respectively.

To describe the trajectory of motion in a static field of central forces $U(r)$, we can write the expression (4) and,
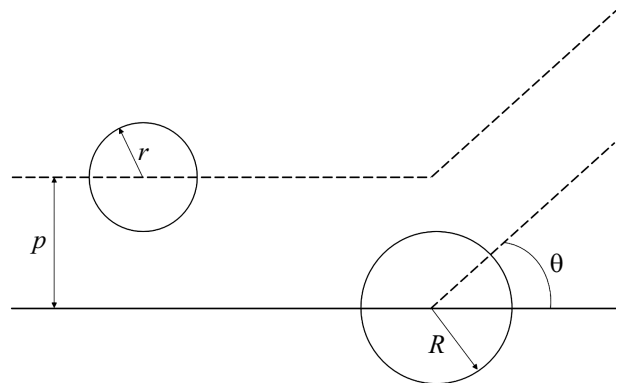
Figure 1. Scattering of two particles in a laboratory coordinate system.

integrating along the entire path, we obtain the equation of motion of the system:

$$\Theta = \pi - \int_{-\infty}^{+\infty} \frac{p\,dr}{r^2\left(1 - \frac{U(r)}{E_{kin}} - \left(\frac{p}{r}\right)^2\right)^{1/2}}, \qquad (4)$$

E_{kin} — kinetic energy of the center of mass, p — sighting parameter, and r — distance between particles. In the case of a spherically symmetric field and provided that the moment and energy of the system are conserved, the resulting equation describes the motion of particles fairly accurately.

As part of this study, a three-dimensional mechanical model of physical sputtering of an amorphous one-component target is considered, where the target has a surface whose map is given from atomic force microscopy (AFM) measurements. The resulting AFM frame is translated into a matrix of numbers and read by the program.

The proposed model uses a number of assumptions that simplify calculations:

— the target in question is amorphous;

— only paired collisions are taken into account;

— elastic and inelastic energy losses are considered separately, and inelastic losses are considered continuous. The model of continuous electronic braking considers the passage of a particle in an electron cloud. Losses occur mainly due to the excitation of weakly bound valence or free electrons. And it is almost not scattered by electrons due to the large mass difference. In this case, it can be assumed that the ion is affected by a continuous braking force directed in the opposite direction;

— such elastic collisions are discretely taken into account in which the transfer of the energy of motion by the particle to the target atom exceeds a certain threshold binding energy E_d. For each test, either a stop (i.e., lying at a depth), or the transfer of momentum to the target atom is recorded, and then the fate of this recoil atom is considered, or scattering. Atomized is considered to be an atom that has crossed the boundary set at the beginning by the coordinate z_0, taking into account the exit energy from the surface;

— The model is statistical in nature based on the Monte Carlo method. The stochastic behavior of the approach gives confidence to the calculations.

The approach implies the „model of atomic billiards", where the Coulomb-type potential is used, taking into account the shielding (7), and the braking capacity is calculated according to the Lindhard–Scharf–Shiott (LSH) model [5]:

$$V(r) = \frac{Z_1 Z_2 e^2}{r} \Phi\left(\frac{r}{a}\right) = \frac{Z_1 Z_2 e^2}{a(r/a)} \Phi\left(\frac{r}{a}\right) = \frac{C}{r/a} \Phi\left(\frac{r}{a}\right), \qquad (5)$$

where Z_1, Z_2 — charges of interacting particles, e — electron charge, a — screening length, $\Phi(r/a)$ — screening function.

The Thomas–Fermi a screening length has the following form:

$$a = \left(\frac{9\pi^2}{128}\right) a_B Z_{12}^{-1/3} = 0.88534 a_B Z_{12}^{-1/3}, \qquad (6)$$

where a_B — represents the Bohr radius, $Z_{12} = (\sqrt{Z_1} + \sqrt{Z_2})^2$ — effective Firsov charge [6].

The screening function $\Phi(r/a)$ is approximated by the expression for solid balls:

$$\Phi(r/a) = \begin{cases} 1 - \dfrac{r}{a}, & r < p \\ 0, & r > p \end{cases}. \qquad (7)$$

The maximum aiming parameter is calculated

$$p_{\max} = \frac{1}{2\sqrt[3]{N}}, \qquad (8)$$

where N — the atomic density of the target in Å^{-3}.

Average free run length:

$$\bar{L} = \frac{1}{\pi r^2 N}, \qquad (9)$$

where r is the radius of the target atom. And the Lindhard constant:

$$K = \frac{1.22 Z_i^{7/6} Z \cdot N}{(Z_i^{2/3} + Z^{2/3})^{3/2} \cdot m_i^{1/2}}, \qquad (10)$$

where Z_i is the charge number of the ion, Z is the charge number of the target atom, m_i is the atomic mass of the ion.

The algorithm of the program boils down to the following.
1) Setting the initial kinetic energy and the initial position of the ion (z_0 and φ). The initial position is set by drawing random coordinates x_0, y_0, which are assigned the corresponding z_0.
2) The free path length of the ion is drawn before the first collision with the target atom:

$$L = -\bar{L} * \ln(\text{Random}). \qquad (11)$$

3) Calculation of z-coordinates of the first collision:

$$z = z_0 + L \cos\varphi. \qquad (12)$$

4) Definition of E_1 ion before the first collision:

$$E_1 = \left(\sqrt{E} - \frac{1}{2} KL\right)^2. \qquad (13)$$

If the expression in parentheses is less than 0 — the ion did not have enough energy, and it stopped at $z < L$, and the coordinate z is calculated:

$$z = z_0 + \left(\frac{2\sqrt{E}}{K} - L\right) \cos\varphi. \qquad (14)$$

If the expression in parentheses is greater than 0, in this case, the algorithm starts with p. 2 for the primary recoil atom (PRA).

5) The aiming parameter for the first collision is drawn by comparing two random numbers in the range $(-1; +1)$:

$$p = p_{\max} \text{Max}(\text{Random}; \text{Random}). \qquad (15)$$

6) Calculation of the energy E_2 of an ion after the first collision in the laboratory coordinate system (SC), i.e. through the masses of ions and targets, taking into account the angle of deviation during the collision in the center of mass system:

$$E_2 = \frac{(\frac{m}{m_i})^2 + 2\frac{m}{m_i}\cos\theta + 1}{(1 + \frac{m}{m_i})^2} E_1, \qquad (16)$$

where θ — the angle of deviation in the center of mass system, which is determined by numerical integration of the expression (4) (integration is implemented by the trapezoid method), where the value of $r_{\min}$ is taken from the solution of the equation $g(r, U) = 0$, where

$$g(r, U) = \sqrt{1 - \frac{p^2}{r^2} - \frac{U(r)}{E_t}}. \qquad (17)$$

7) The angles θ_i and θ_a between the ion, atom and the axis y to the direction of departure of the ion after the first collision in the laboratory are determined (Fig. 2):

$$\theta_i = \frac{\text{arctg}(\sin\theta)}{\cos(\theta) + \frac{m}{m_i}}, \qquad (18)$$

$$\theta_a = \frac{\pi}{2}_\theta. \qquad (19)$$

8) Drawing of the deflection angle of the χ ion at the first collision:

$$\chi = 2\pi\text{Random}, \qquad (20)$$

9) The angle φ between the ion and the axis z to the direction of departure of the ion after the first collision in the laboratory is determined:

$$\cos\varphi_1 = \cos\varphi\cos\psi + \cos\chi\sin\varphi\sin\psi, \qquad (21)$$

where

$$\cos\psi = \frac{1 + \frac{m}{m_i}\cos\theta}{\sqrt{(\frac{m}{m_i})^2 + 2\frac{m}{m_i}\cos\theta + 1}}. \qquad (22)$$

10) For each map, the critical angle a_c is calculated, which is the angular size of the partition grid cell. The critical angle and the scattering angle are compared. If the obtained angle is greater than the critical one, then the algorithm of transition to other coordinates x, y and z is started (Fig. 3)

$$\alpha_c = 2\arctg\frac{x_n - x_{n-1}}{2(z_{n-1} - z_n)}. \qquad (23)$$

11) The recoil atom energy is calculated:

$$E_a = E_e - E_2 - E_d. \qquad (24)$$
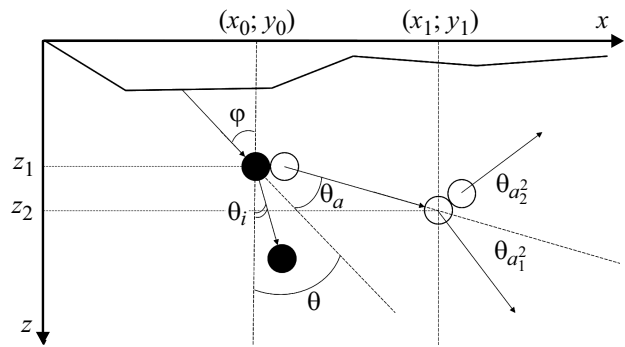
Figure 2. Schematic representation of the collision cascade.
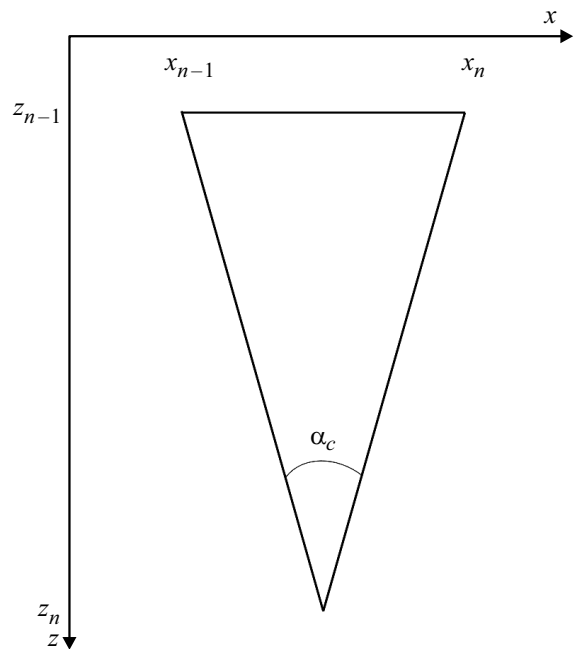
Figure 3. The angular size of the calculated cell.

12) Items from 2 to 11 are performed as long as the ion energy exceeds the binding energy value for this material $(E > E_d)$. For each recoil atom, an internal cycle similar to the one described above is started. Thus, this model implements a description of linear interaction cascades up to and including recoil atoms of the third order. When this event has occurred, the current loop is closed and the next iteration is calculated, i.e. item 1, 2.

13) Atomized is the atom that crossed the initial coordinate z_0. The number of incoming ions is set using the keyboard and, since the value of Y is determined by the expression (1), the more ions are set, the more sampling occurs, and the more fair the value of the sputtering coefficient will be.

14) Next, taking into account the obtained values, the final surface map is calculated according to (25) and subtracted from the original:

$$\text{Surface}[x, y] = Y \cdot N \cdot k[x, y], \qquad (25)$$

where N is the atomic density of the substance, and $k[x, y]$ is the map of the number of drops of the corresponding coordinate.

To obtain correct results of calculations of the spray coefficients, it is necessary to conduct one experiment on ion etching, from which the correction factor d is determined. In then the expression (1) will be rewritten taking into account this coefficient:

$$Y = \delta \frac{Count\ of\ ejected\ atoms}{Count\ of\ incident\ particles}. \quad (26)$$

2. Calculation of surface roughness

The resulting surface map Surface$[x, y]$, as well as the data obtained by the AFM method, is a discrete map of the set of heights $z(\boldsymbol{\rho})$, where $\boldsymbol{\rho} \equiv (x, y)$. Using the obtained maps, two-dimensional PSD functions (spectra of heterogeneities in lateral size on the surface) can be constructed, which are given by a two-dimensional Fourier transform from the autocorrelation function (28):

$$\text{PSD}_{2D}(\boldsymbol{\nu}) = \int \exp(2\pi i \boldsymbol{\nu} \boldsymbol{\rho}) C(\boldsymbol{\rho}) d\boldsymbol{\rho}, \ \ \boldsymbol{\nu} \equiv (\nu_x, \nu_y), \quad (27)$$

where $\boldsymbol{\nu}$ is the spatial frequency vector, and the correlation function $C(\boldsymbol{\rho})$ is defined as:

$$C(\boldsymbol{\rho}) = \left\langle z(\boldsymbol{\rho} + \boldsymbol{\rho}') z(\boldsymbol{\rho}) \right\rangle, \ \ \boldsymbol{\rho} \equiv (x, y). \quad (28)$$

Knowing the PSD function, it is possible to calculate the value of the effective surface roughness by integrating over spatial frequencies:

$$\sigma_{\text{eff}}^2 = 2\pi \int_{\boldsymbol{\nu}_{\min}}^{\boldsymbol{\nu}_{\max}} \text{PSD}_{2D}(\boldsymbol{\nu}) \boldsymbol{\nu} d\boldsymbol{\nu}. \quad (29)$$

The model was tested on samples of amorphous silicon deposited by magnetron sputtering on standard silicon substrates.

3. Experiment description

Amorphous silicon films (thickness 500 nm) deposited by magnetron sputtering on standard polished substrates of monocrystalline silicon $(1\,0\,0)$ for the microelectronic industry were used as samples [7].

As a source of accelerated ions, a Kaufman-type technological source with a cold cathode KLAN-104M (NTK „Platar") was used. To conduct the experiment, the sample is mounted on a slide table and the required angle of inclination relative to the normal is set, while part of the surface is covered with a mask to control the removal or a „witness grqq is used. Further, a working gas pressure of the order of $1.3 \cdot 10^{-2}$ Pa is created in the chamber. Further, the necessary ion current density (j) and

accelerating voltage ($U_{\text{acc.}}$) are set. The sample is subjected to ion bombardment, after which the etching depth and surface roughness are measured.

The etching depth is measured using a white light interference microscope Talysurf CCI 2000. The height of the formed step is measured.

From the measured values of the etching depth, knowing the time, the value for the etching rate V_{etch} was calculated. Since V_{etch} is proportional to the ion sputtering coefficient, having determined this proportionality, it is possible to calculate the values for Y. Taking as a basis the definition of the sputtering coefficient, by small transformations we obtained the expression (30) for Y, where the input data are the parameters of the experiment:

$$Y = \frac{\rho \, e V_{etch} N_A}{\cos \Theta_{in} j M_2}, \quad (30)$$

where ρ — target density, N_A — Avogadro number, Θ_{in} — angle of incidence of ions on the surface, j — ion current density, M_2 — molar mass of the target, V_{etch} — etching rate.

The RMS roughness is measured on an Ntegra probe microscope (NT-MDT), in the range of spatial frequencies (q) $7.81 \cdot 10^{-3} - 6.25 \cdot 10^{-2}$ nm^{-1} (frame size 128×128 nm^2).

The roughness was calculated using the method described above.

4. Results and discussions

4.1. Study of spray coefficients

The study of the sputtering coefficients was reduced to obtaining the dependences of the etching rate on the energy of the incoming ions under normal line, as well as removing the dependence of the etching rate on the angle at a fixed energy. The obtained velocity values were recalculated according to the formula (29) into the values of the spray coefficients.
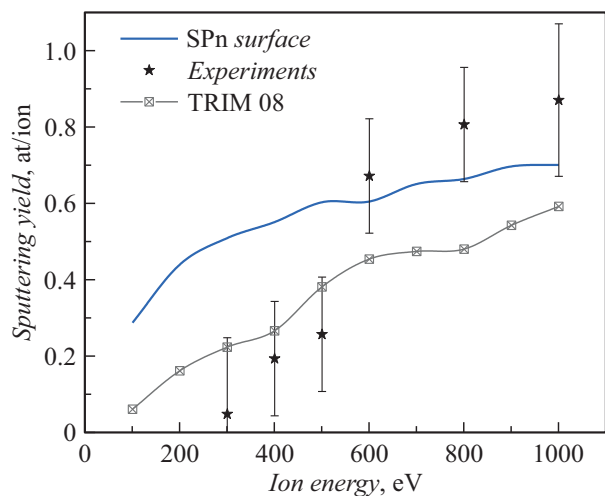
Figure 4. The dependence of the Si sputtering coefficient on the energy of the Ar ions.
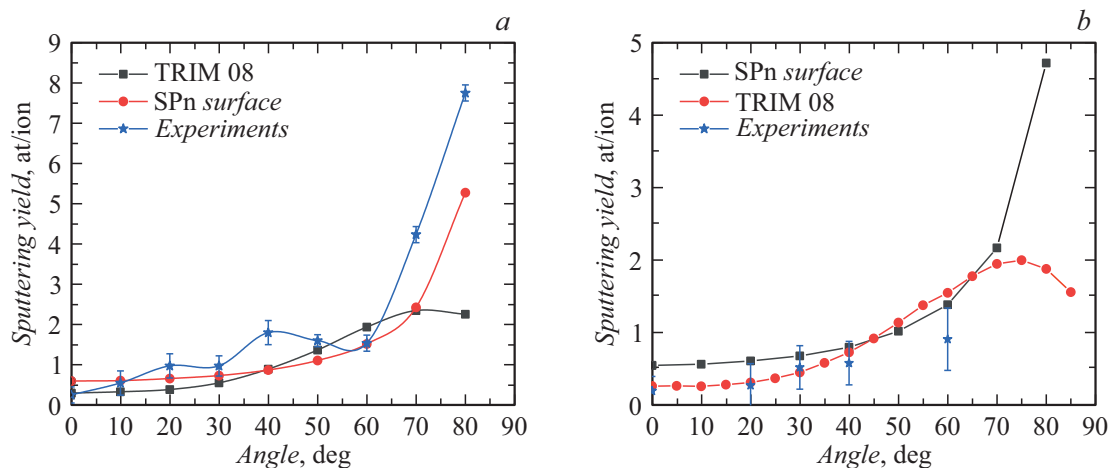
Figure 5. Angular dependences of the sputtering coefficient of amorphous silicon by Ar ions with an energy of 500 (*a*) and 400 eV (*b*).

Fig. 4 shows the dependences of the sputtering coefficients for an amorphous silicon target irradiated with accelerated argon ions on the energy and angle of incidence.

The figure shows that the resulting dependence, in this energy range $(0-1000 \, \text{eV})$, has the form of a monotonically growing curve. Moreover, the curve calculated in TRIM [8] has a similar form. However, at energies less than 600 eV, the experimental points lie noticeably lower than the calculated ones. Such an underestimated value may be due to the fact that there is always a small layer of oxide film on the surface of the sample, which sprays more slowly and, as a result, introduces inaccuracy in the determination of the sputtering coefficient [9], which has a much greater effect when spraying with low energies. However, the obtained values at energies above 600 eV are in better agreement with the experiment than the simulation results in the TRIM [8] package.

Fig. 5 shows the results of numerical simulation of the angular dependence of the sputtering coefficient for a silicon film irradiated with argon ions with an energy of 500 and 400 eV.

As can be seen from Fig. 5, the type of calculated angular dependences of the sputtering coefficient repeats the behavior of the analytical and experimental dependences [10], however, a discrepancy is observed quantitatively. A good agreement of the results with the experiment is observed in the range of angles up to 60 degrees.

4.2. Study of the evolution of the surface of amorphous silicon under the action of ion beam etching

The study of the evolution of the surface of amorphous silicon under the action of ion beam etching was carried out by studying the spectral characteristics (PSD functions) obtained from AFM data. By analogy, maps of irradiated surfaces were obtained, for each of which PSD functions were subsequently constructed.
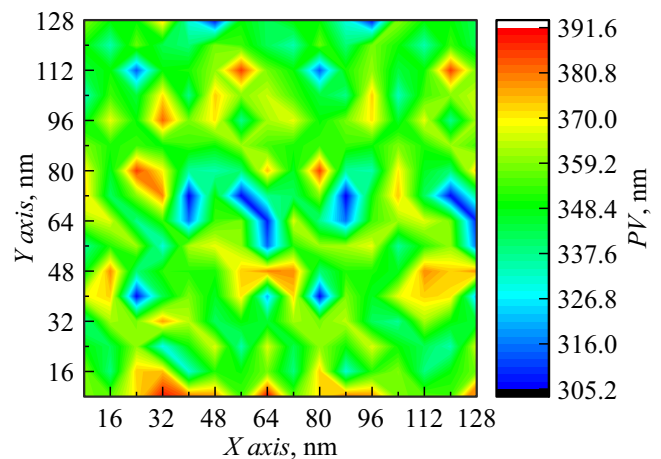
Figure 6. Map $128 \times 128 \, \text{nm}^2$ of the original surface Si, $\sigma_{\text{eff}} = 0.34 \, \text{nm}$.

Below are maps of silicon film surfaces before (Fig. 6) and after numerical simulation (Fig. 7).

After simulating the irradiation of the Si surface with Ar ions with an energy of 800 eV under normal line, the effective roughness decreased to the value $\sigma_{\text{eff}} = 0.31 \, \text{nm}$ in the spatial frequency range $7.81 \cdot 10^{-3} - 6.25 \cdot 10^{-2} \, \text{nm}^{-1}$. Etching at an angle is often accompanied by the development of relief and the formation of artifacts on the surface, which leads to a deterioration of roughness [11]. In our case, etching with argon ions with an energy of 800 eV at an angle of 60 deg to the surface was simulated, as a result of which the value of the effective roughness increased to 0.37 nm.

To test the model, a number of experiments were carried out with the same values of the energies and angles of incidence of ions on the sample surface. Below are a pair of AFM frames $128 \times 128 \, \text{nm}^2$ of the initial and irradiated surfaces (Fig. 8, 9).

The spectral characteristics of the surfaces subjected to ion bombardment are given below (Fig. 10).
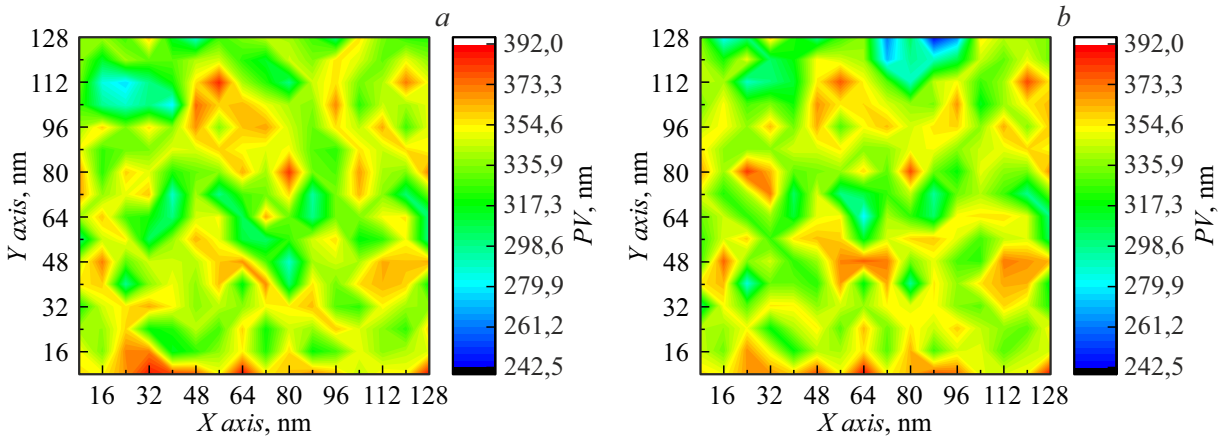
Figure 7. Map $128 \times 128 \, \text{nm}^2$ etched surface Si by Ar ions: a —$E_{ion} = 800 \, \text{eV}$, $\varphi = 0°$ 2000 iterations; $\sigma_{\text{eff}} = 0.31 \, \text{nm}$; b — $E_{ion} = 800 \, \text{eV}$, $\varphi = 60°$, 2000 iterations, $\sigma_{\text{eff}} = 0.37 \, \text{nm}$.
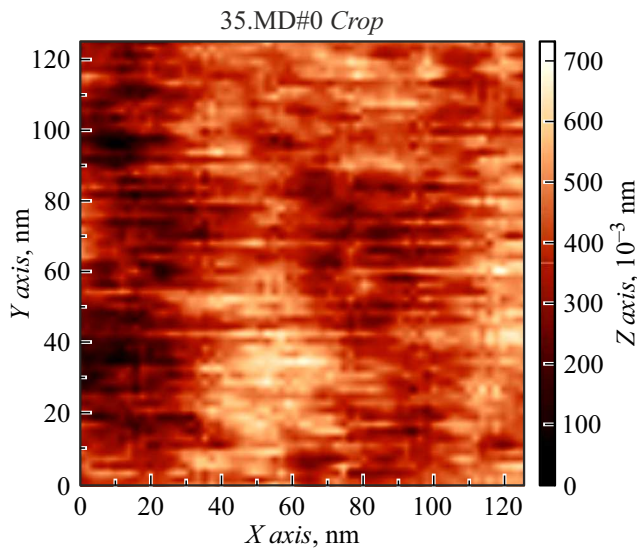
Figure 8. AFM frame $128 \times 128 \, \text{nm}^2$ of the original surface of amorphous Si with $\sigma_{\text{ef}} = 0.34 \, \text{nm}$.
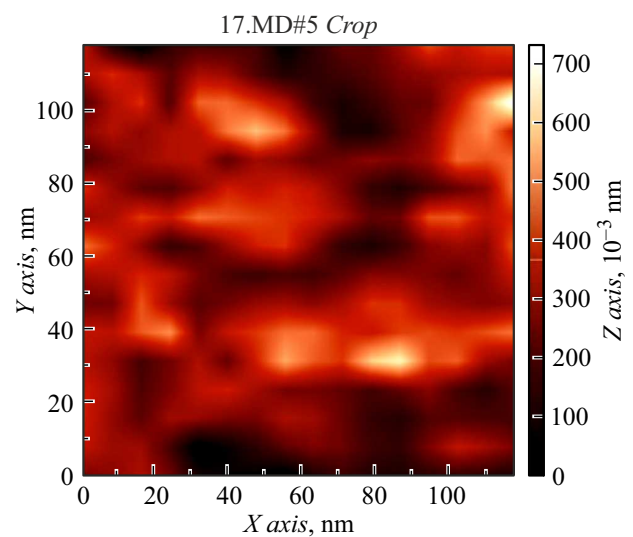
Figure 9. AFM frame $128 \times 128 \, \text{nm}^2$ etched surface Si by Ar ions with energy 800 eV at an angle of 60 deg. $\sigma_{\text{ef}} = 0.42 \, \text{nm}$.

The sample Si#1 corresponds to the initial surface; Si#2 — irradiated with argon ions with an energy of 800 eV at an angle of 60 deg; Si#3 — irradiated with argon ions with an energy of 800 eV under normal line. It can be seen that after etching under normal line, a smoothing effect is observed in the entire range of spatial frequencies, while the development of the relief is manifested at an angle (the blue curve (in the online version) in the area of medium and low spatial frequencies lies above the original one). Thus, the value of the effective roughness was improved by 20% when etching under normal line, while at an angle of 60 deg, this value deteriorated by 23% relative to the original.

Also, to check the effectiveness of the program, the minimum number of iterations was estimated to obtain a reliable value of the spray coefficient (Fig. 11). The dotted line in the figure indicates the desired value. It can be
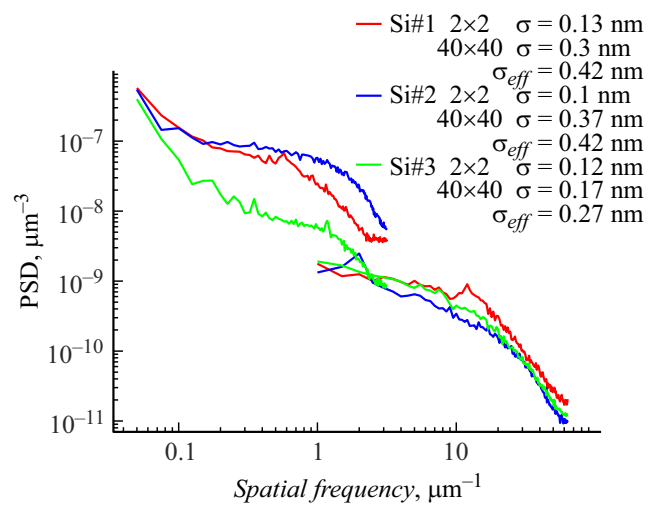
Figure 10. PSD-functions of Si surfaces bombarded by accelerated Ar ions with an energy of 800 eV.
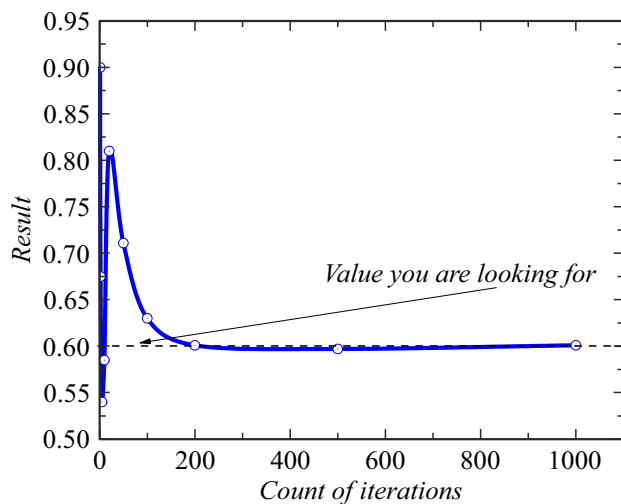
Figure 11. Dependence of the output value of the spray coefficient on the number of iterations.

seen that, starting from 200 iterations, the value of the spray coefficient changes in the second and third decimal places.

Conclusion

Thus, the paper demonstrates a pulsed mechanism of physical sputtering taking into account the evolution of the surface on the example of our SPnSurface algorithm. The results of numerical simulation qualitatively coincide with those observed in experiments. Moreover, for amorphous silicon irradiated with accelerated argon ions, the calculated values of the sputtering coefficient from the energy are in good agreement with the experiment at energies above 600 eV. The angular dependences quantitatively coincide with the experiment in the range of angles up to 60 deg. Further, there is a discrepancy in values up to 40% of those obtained experimentally. It is worth noting that TRIM at angles above 60 deg shows a deviation of up to 70% relative to the values obtained in the experiment. The difference in values can be explained by the amount of material removal. In all experiments, the etching depth was 100 nm, while in the simulation, due to the long calculation times, the removal value was about ten angstroms.

Conflict of interest

The authors declare that they have no conflict of interest.

References

[1] M.S. Mikhailenko, N.I. Chkhalo, S.A. Churin, M.A. E. Pestov, V.N. Polkovnikov, N.N. Salashchenko, M.V. Zorina. Appl. Opt. **55** (6), 1249–1256, (2016). https://doi.org/10.1364/AO.55.001249

[2] X. Li, D. Wang, F. Nie, P. Wu, Sh. Zhao. 10th International Symposium on Advanced Optical Manufacturing and Testing Technologies: Advanced and Extreme Micro-Nano Manufacturing Technologies. 120730L (2021). https://doi.org/10.1117/12.2605262

[3] Wen Hui Deng, Xian Hua Chen, Hui Liang Jin, Bo Zhong, Jin Hou, An Qi Li. Young Scientists Forum 2017. 107102W (2018). https://doi.org/10.1117/12.2316623

[4] P. Sigmund. Phys. Rev., **187**, 768 (1969). https://doi.org/10.1103/PhysRev.184.383

[5] J. Lindhart, M. Scharff, H. Schiott. Mat. Fys. Medd. Dan. Vid. Selsk., 33 (1963).

[6] O.B. Firsov. Zh. Eksp. Teor. Fiz., (1957).

[7] [Electronic resource] Available at: http://www.telstv.ru/?page=en_silicon_wafers

[8] J.F. Ziegler, M.D. Ziegler, J.P. Biersack. Nucl. Instrum. Methods Phys. Res. B, **268** (11−12), 1818–1823 (2010). https://doi.org/10.1016/j.nimb.2010.02.091

[9] Y.A. Vainer, M.V. Zorina, A.E. Pestov, N.N. Salashchenko, N.I. Chkhalo, R.A. Khramkov. Bull. Russ. Academ. Sci.: Phys., **75** (1), 61–63 (2011). DOI: 10.3103/S1062873811010254

[10] Qiangmin Wei, Kun-Dar Li, Jie Lian, Lumin Wang. J. Phys. D: Appl. Phys., **41**, 172002 (2008). DOI: 10.1088/0022-3727/41/17/172002

[11] M. Karlušić, M. Mičetić, M. Kresić, M. Jakšić, B. Šantić, I. Bogdanović-Radović, S. Bernstorff, H. Lebius, B. Band'Etat, K. Žužek Rožman, J.H. O'Connell, U. Hagemann, M. Schleberger. Appl. Surf. Sci., **541**, 148467 (2021). https://doi.org/10.1016/j.apsusc.2020.148467